HOKKAIDO UNIVERSITY

Title	Chemical stability of porous anodic aluminum oxide in both acidic and alkaline solutions
Author(s)	Iwai, Mana; Kikuchi, Tatsuya
Citation	Thin solid films, 771, 139784 https://doi.org/10.1016/j.tsf.2023.139784
Issue Date	2023-04-30
Doc URL	https://hdl.handle.net/2115/94186
Rights	© <2023>. This manuscript version is made available under the CC-BY-NC-ND 4.0 license http://creativecommons.org/licenses/by-nc-nd/4.0/
Rights(URL)	https://creativecommons.org/licenses/by-nc-nd/4.0/
Type	journal article
File Information	107780.pdf

Hokkaido University Collection of Scholarly and Academic Papers : HUSCAP

Chemical stability of porous anodic aluminum oxide in both acidic and alkaline solutions

Mana Iwai, Tatsuya Kikuchi*
Faculty of Engineering, Hokkaido University, N13-W8, Kita-ku, Sapporo, Hokkaido, 060-8628, Japan

*Corresponding author: Tatsuya Kikuchi
e-mail: kiku@eng.hokudai.ac.jp

Abstract

A porous anodic aluminum oxide (AAO) possessing higher chemical resistance in both acidic and alkaline solutions was fabricated by anodizing Al in an alkaline sodium tetraborate solution. The 5N Al plates were anodized in five types of major acidic solutions (sulfuric, oxalic, phosphoric, chromic, and etidronic acids) and in alkaline sodium tetraborate solution to form AAOs. The anodized specimens were then immersed in a 0.52 M phosphoric acid solution (pH = 1.3) and a 2.5 M sodium hydroxide solution (pH = 13.8). Subsequently, the electrochemical impedance measurements and morphological characterizations of the AAOs before and after immersion were investigated. The time required for the complete dissolution of the AAOs formed in typical acidic electrolytes, including sulfuric, oxalic, phosphoric, and etidronic acids, increased linearly with the anodizing voltage. The AAO formed in chromic acid exhibited a higher chemical resistance than this linear relationship owing to the formation of high-purity alumina without incorporated anions. Moreover, the AAO formed in sodium tetraborate exhibited the highest chemical resistance in both acidic and alkaline solutions – approximately two times higher than that formed in etidronic and chromic acids. This can be attributed to their higher anodizing ratio and the formation of a high-purity alumina layer.

Keywords: Anodizing Aluminum; Porous Oxide Film; Sodium Tetraborate, Chemical Resistance

1. Introduction

Al and its alloys are now used in various industrial applications, such as automobiles, trains, airplanes, building materials, electronic products, and household items. Because bare Al is easily corroded in corrosive environments (e.g., acidic, alkaline, and chloride-containing aqueous solutions), surface finishing is typically required for the corrosion protection of various Al products. Electrochemical anodizing is one of the most important surface finishing methods for Al [1-10]. This process causes the formation of a corrosion-resistant porous anodic aluminum oxide (AAO) consisting of an outer honeycomb porous layer and an inner thin barrier alumina layer on the Al surface [11-15]. AAO can generally be obtained by anodizing in appropriate acidic solutions, such as sulfuric acid (H_2SO_4) [16-18], oxalic acid ($(COOH)_2$) [19-21], phosphoric acid (H_3PO_4) [22-24], chromic acid (H_2CrO_4) [25-27], and etidronic acid ($C_2H_8O_7P_2$) [28-30]. Among these electrolytes, sulfuric acid is widely used in industrial anodizing processes because of its low cost, low applied voltage, and transparency of the obtained AAO. However, the use of chromic acid solution containing Cr^{6+} has been avoided for safety related reasons in recent years despite the AAO obtained by anodizing in chromic acid possessing a high corrosion resistance. The type of electrolyte species used during anodizing strongly affects the nanomorphology and chemical composition of the AAOs [31,32]. For example, the appropriate anodizing voltage for the uniform growth of AAO varies greatly depending on the type of electrolyte used, and the thickness of the barrier alumina layer formed at the bottom of the AAO increases linearly with the anodizing voltage [33]. In addition, electrolyte anions, such as SO_4^{2-} and PO_4^{3-}, are incorporated into anodic alumina during anodizing in many cases. Thus, AAOs containing small amounts of electrolyte anions are obtained [34-37]. Different morphologies and chemical compositions of AAOs strongly affect the corrosion resistance of AAO-covered Al [38,39].

We reported that anodizing Al in several alkaline solutions, such as sodium tetraborate ($Na_2B_4O_7$) and sodium metaborate ($NaBO_2$), results in the fabrication of AAOs possessing characteristic nanomorphologies on the Al surface [40-44]. For example, a highly ordered AAO, with a wide range of cell sizes (interpore distance) measuring 260–590 nm, grows under an unconventional self-ordering regime via anodizing in sodium tetraborate. This anodizing allows the uniform formation of an ordered pore structure without the occurrence of burning on various complicated three-dimensional Al surfaces. A unique AAO, possessing an ultra-flat barrier layer and extremely high porosity, was fabricated by anodizing in sodium metaborate. More recently, we reported the anodizing behaviors in phosphoric acid and six types of phosphate solutions with a wide pH range from acidic to alkaline [45]. Two types of unique AAO films were formed in alkaline phosphate solutions: one was a AAO film consisting of an outer porous layer possessing feathered pore walls and inner hemispherical barrier layer, and the second was a AAO film consisting of an outer porous layer with narrow pores and inner flat barrier layer. During the anodizing of Al in these alkaline solutions, we found that high-purity AAO with a thick barrier layer was formed on the Al surface. Therefore, such anodizing in alkaline solutions may lead to higher corrosion resistance of Al.

Recently, chemical-resistant coating methods are required for the corrosion protection of aluminum in various industries [46-48]. In this study, we describe an AAO, formed by anodizing

in sodium tetraborate, exhibiting a higher chemical resistance in both acidic and alkaline solutions. The AAOs were obtained by anodizing in five typical acidic electrolyte solutions (sulfuric, oxalic, chromic, phosphoric, and etidronic acids) and also in an alkaline electrolyte solution (sodium tetraborate). Subsequently, these AAO-covered Al specimens were immersed in phosphoric acid and sodium hydroxide (NaOH) solutions to evaluate their chemical resistance. The electrochemical measurements and morphological characterizations of the AAOs before and after immersion were investigated in detail. It was found that the AAO film formed in sodium tetraborate possessed a higher chemical resistance than the conventional AAOs formed in typical acidic electrolytes.

2. Experimental

Commercially available Al plates (99.999 wt%, 2 cm × 1 cm with an electroconductive part, 500 μm thick, Nippon Light Metal, Japan) were ultrasonically washed in 99.5 wt% ethanol for 10 min. The bottom half of the electroconductive part was covered with a silicone resin to fix the anodizing area after ultrasonication. The Al specimen as the anode and a large Al plate as the cathode were immersed in a mixture of 22 vol% perchloric acid ($HClO_4$, 70 wt% solution) and 78 vol% acetic acid (CH_3COOH) at 280 K, and potentiostatic electropolishing was carried out at 28 V for 2 min.

The pre-treated Al specimens were immersed in five types of acidic electrolyte solutions – 0.3 M sulfuric acid (293 K), 0.3 M oxalic acid (293 K), 0.3 M phosphoric acid (293 K), 0.3 M chromic acid (313 K), and 0.3 M etidronic acid (313 K). They were also immersed in an alkaline electrolyte solution – 0.3 M sodium tetraborate (333 K). The Al specimens were then anodized at a constant current density of 40 Am^{-2} for 60 min using a high-precision power supply (MODEL 6911, Metronix, Japan). Constant-current anodizing in sulfuric acid, oxalic acid, and phosphoric acid was carried out at 293 K, whereas the anodizing in chromic acid, etidronic acid, and sodium tetraborate was performed at relatively higher temperatures in the range of 313–333 K to avoid oxide burning. The temperature of the electrolyte solution was adjusted using a water bath (UCT-1000, AS ONE, Japan) and the solution was stirred using an underwater magnetic stirrer (Thermo Scientific, iMicroStirrer, USA). Voltage–time curves during galvanostatic anodizing were measured using a digital multimeter (VOAC7602, IWATSU, Japan). The AAOs formed by anodizing in sulfuric acid, oxalic acid, phosphoric acid, chromic acid, etidronic acid, and sodium tetraborate solutions are denoted as Sul-AAO, Oxa-AAO, Phos-AAO, Chro-AAO, Eti-AAO, and Borate-AAO, respectively.

The AAO-covered Al specimens were immersed in a 0.52 M phosphoric acid solution at 333 K (pH = 1.3) and a 2.5 M sodium hydroxide solution at 293 K (pH = 13.8) for up to 50 min to investigate the dissolution behavior of AAO in acidic and alkaline solutions. The volume of the electrolyte solution was adjusted to 100 mL and the Al specimens were maintained in static electrolyte solutions without stirring.

The depth profiles of the elements contained in the AAOs were analyzed using glow discharge optical emission spectrometry (GD-OES, JY-5000RF, HORIBA, Japan). The nanostructural changes in the surface and fracture cross-sections of the AAOs before and after

immersion in phosphoric acid and sodium hydroxide solutions were observed using scanning electron microscopy (SEM, TM-1000, Hitachi High-Technologies, Japan, operating voltage: 15 kV, and JSM6500F, JEOL, Japan, operating voltage: 10 kV). In addition, high-magnification images of the vertical cross-section of the AAOs and the corresponding elemental distribution were obtained using Cs-corrected scanning transmission electron microscopy (STEM, Titan3 G2 60-300, FEI, USA, operating voltage: 300 kV) and energy dispersive X-ray spectroscopy (EDS). For STEM observations, the Al specimens were sliced to a thickness of 25 nm by ultramicrotomy (Powertome XL, RMC, USA) using a diamond knife, and then the ultra-sectioning specimens were placed on a Cu mesh grid with a support film. The structural changes in the AAOs were also investigated using electrochemical impedance spectroscopy (EIS, CompactStat.h10800, Ivium, Netherlands). For EIS measurements, the Al specimens were immersed in a neutral 0.5 M boric acid (H_3BO_3)/0.05 M sodium tetraborate solution (pH = 7.4). The impedance spectra were then measured at the open circuit potential (OCP) using a 10 mV amplitude sinusoidal alternating voltage in the frequency range of 10^{-1} to 10^5 Hz.

3. Results and Discussion

The pre-treated Al specimens were galvanostatically anodized in five types of acidic electrolytes including 0.3 M sulfuric, oxalic, phosphoric, chromic, and etidronic acid solutions, and a 0.3 M alkaline sodium tetraborate solution at a constant current density of 40 Am^{-2} for 60 min to form AAO on the Al surface. Fig. 1 shows the changes in the anodizing voltage (U_a) with time (t_a) during each galvanostatic anodizing process. A region of linear voltage increase was observed during the initial stage of anodizing. The voltage increase rates obtained in typical acidic electrolytes, such as sulfuric, oxalic, phosphoric, and etidronic acids, were measured to be 60–70 $Vmin^{-1}$. These rates were higher than those obtained in chromic acid (43 $Vmin^{-1}$) and sodium tetraborate (40 $Vmin^{-1}$). In addition, the voltage-time curve for all the acids (except chromic acid) exhibited a maximum value before reaching the steady-state voltage. For chromic acid, the voltage reached the steady state without any peak. As a result, the voltages during each galvanostatic anodizing process reached a steady-state value after the initial stage: 16 V in sulfuric acid, 35 V in oxalic acid, 103 V in chromic acid, 129 V in phosphoric acid, 142 V in etidronic acid, and 190 V in sodium tetraborate. It is widely accepted that the thickness of the barrier layer formed at the bottom of AAOs increases in proportion to the anodizing voltage despite the varying proportionality constant being dependent on the type of electrolyte used (typical acidic electrolyte: 1.05 nmV^{-1}, sodium tetraborate: 1.38 nmV^{-1}) [40]. Therefore, anodizing at a higher voltage causes the formation of AAOs with a thicker barrier layer.

Fig. 2 shows the SEM images of the fracture cross-section of the AAO obtained by anodizing in six types of electrolyte solutions at 40 Am^{-2} for 60 min. A AAO with a high aspect ratio and narrow cells measuring approximately 40 nm in cell size was observed after anodizing in sulfuric acid. The barrier layer formed at the bottom of the Sul-AAO was relatively thin, measuring approximately 20 nm owing to the low-voltage anodizing (16 V). The cell size increased with the anodizing voltage, and larger AAOs measuring approximately 80, 290, and 360 nm in cell diameter were obtained by anodizing in oxalic acid (35 V), phosphoric acid (129

V), and etidronic acid (142 V), respectively. In addition, the barrier layer thickness increased to approximately 40 nm for Oxa-AAO, 130 nm for Phos-AAO, and 160 nm for Eti-AAO. These four AAOs possessed a typical nanomorphology consisting of an upper porous layer with smooth pore walls and a lower hemispherical barrier layer. In contrast, the AAOs formed in chromic acid and sodium tetraborate exhibited a characteristic feathered structure on their pore walls. Because the voltage during anodizing in sodium tetraborate (190 V) was considerably higher than that in chromic acid (103 V), the barrier layer thickness of Borate-AAO (approximately 230 nm) was greater than that of Chro-AAO (130 nm). Although the same operating conditions, such as the concentration, temperature, current density, and anodizing time, were employed for each anodizing process, the total thickness of the AAO varied slightly depending on the electrolyte. For example, the thickness of the former four AAOs was approximately 7 μm, while the latter two AAOs were relatively thin at 5 μm. C. V. Thompson et al. suggested that a reduced steady-state growth rate is expected for the AAOs with the feathered structure by suppressing the oxide flow [49]. Anodizing aluminum in chromic acid and sodium tetraborate solutions caused the formation of feathered structure on the pore wall (Fig. 2). Therefore, the thickness of the AAOs formed in chromic acid and sodium tetraborate may be thinner than that of AAOs formed in other four acids.

Fig. 3 shows the GD-OES elemental depth profiles of AAOs formed by anodizing in six types of electrolyte solutions for 60 min, as shown in Fig. 2. Here, the reason why the complete etching time of each AAO layer depends on the type of electrolyte used may be due to the differences on the porosity and hardness of the AAOs formed by anodizing in different electrolytes [30]. Sulfur originating from sulfate anions was present in the entire vertical region of the anodic alumina. Similarly, Oxa-AAO contained C originating from oxalate anions, and Phos-AAO and Eti-AAO contained P originating from phosphate and etidronate anions, respectively. It is widely accepted that electrolyte anions are incorporated into the barrier layer at the bottom of the AAO during these anodizing processes, and the depth of the incorporated barrier layer region depends on the electrolyte used. In addition, the ratio of the anion incorporation thickness to the total thickness decreases with increasing voltage (Sul-AAO > Oxa-AAO > Phos-AAO > Eti-AAO) [50]. In contrast, the Chro-AAO and Borate-AAO consisted of pure alumina without incorporated anions, such as Cr and B, except for the outermost surface. Extremely small amounts of Cr and B measured at the outermost layer of the AAOs are expected due to the adsorption of electrolyte anions onto the alumina surface.

Table 1 summarizes the anodizing behaviors and structural parameters of the AAO fabricated by anodizing in different electrolyte solutions. The differences in the nanomorphology and composition of each AAO, shown in Figs. 2 and 3, are expected to significantly affect the chemical resistance in acidic and alkaline solutions. Therefore, the AAO-covered Al specimens formed by each anodizing process were immersed in phosphoric acid and sodium hydroxide solutions, and then electrochemical measurements and morphological characterizations were performed.

The Al specimens covered with each AAO were immersed in a 0.52 M phosphoric acid solution at 333 K for various periods (t_i) to evaluate their chemical resistance. After immersion,

the impedance Bode diagrams for these Al specimens and the electropolished Al specimen were obtained by EIS in a neutral 0.5 M boric acid/0.05 M sodium tetraborate solution. For example, Fig. 4a shows Bode diagrams for the Al specimen covered with Phos-AAO and the electropolished Al specimen. The experimental and simulated values are represented by solid circles and lines, respectively. A schematic illustration of the corresponding equivalent circuit of AAO formed on the Al surface is shown in Fig. 4b. In this equivalent circuit, R_s is the resistance of the neutral borate solution used for EIS measurements, $(CPE)_b$ is the constant phase element (CPE) for the capacitance of the barrier layer formed at the bottom of the AAOs, and R_b is the resistance of the barrier layer. The impedance of the electropolished Al specimen without AAO consisted of two regions: a slope line at 10^{-1}–10^3 and a horizontal line above the 10^3 region. As the Al surface was covered with Phos-AAO (i.e., $t_i = 0$ without immersion in phosphoric acid after anodizing), the slope line changed to a high impedance value owing to the existence of Phos-AAO on the Al surface. However, the slope gradually changed to a low-impedance value with increasing immersion time in the phosphoric acid solution because of the dissolution of the barrier anodic alumina (t_i = 2-17 min). After prolonged immersion for t_i = 20–22 min, the shape of the Bode diagrams was approximately the same as that of the electropolished Al specimens. This may be due to the complete dissolution of Phos-AAO by immersion in the phosphoric acid solution for more than t_i = 20 min, and the surface became similar to that of electropolished Al without anodic alumina.

The capacitance of the bottom barrier layer was inversely proportional to its thickness. Therefore, changes in the barrier layer thickness after immersion in phosphoric acid can be examined using impedance Bode diagrams. The reciprocal capacitances (C_bs) were calculated using the simulated curve of the Bode diagrams shown in Fig. 4. In addition, the effect of the immersion time in phosphoric acid on the reciprocal C_b of the Phos-AAO-covered Al specimens is summarized in Fig. 5. The reciprocal C_b before immersion in phosphoric acid solution was measured to be 16.7 $cm^2\mu F^{-1}$. After immersion, the reciprocal of C_b decreased with increasing immersion time because of the dissolution of the anodic alumina barrier layer in the phosphoric acid solution. Furthermore, the value became almost zero after immersion for approximately 20 min. The slopes of the linear time variation of reciprocal C_b obtained in the first and second half periods of immersion were clearly different (-1.09 and -0.65 $cm^2\mu F^{-1}$ min^{-1}). This corresponds to a change in the dissolution rate of Phos-AAO during the immersion process. Structural characterizations of the vertical cross-section of these Phos-AAO-covered Al specimens before and after immersion in phosphoric acid were performed using SEM and STEM.

Fig. 6a shows SEM images of the top surface and fractured cross-section of the Phos-AAO after immersion in phosphoric acid solution for a period of 7–20 min. Compared with the SEM image of the Phos-AAO before immersion shown in Fig. 2, the thickness of the barrier layer decreased and the diameter of the pores increased after immersion in phosphoric acid for 7 min because of the dissolution of anodic alumina. The barrier layer thinning and pore widening progressed after long-term immersion, and narrow pore walls and barrier layers were observed after immersion for 17 min. Thus, the reciprocal of C_b shown in Fig. 5a also decreased with

increasing immersion time. After further immersion for 20 min, slight fibrous alumina structures were obtained on the exposed dimpled Al surface; thus, the C_b value was almost zero.

Fig. 6b shows the STEM-EDS elemental distribution maps of Al, O, and P in Phos-AAO before and after immersion in phosphoric acid. The red, blue, and yellow colors shown in the maps indicate the distributions of Al, O, and P, respectively. The barrier layer and pore walls of the Phos-AAO possessed a two-layer structure: an outer alumina layer containing P, which originates from the incorporated phosphorus anions, and an inner pure alumina layer without anions. As Phos-AAO was immersed in the phosphoric acid solution, the barrier alumina layer dissolved gradually from its outermost surface. Although the outer alumina layer containing P remained after immersion for 7 min, this outer layer was completely dissolved after further immersion for 15 min. In addition, the inner barrier alumina layer without anions was only observed on the Al surface. The reason for the change in the dissolution rate of Phos-AAO shown in Fig.5 was the presence or absence of phosphorus anions in the anodic alumina layer. Because the dissolution rate of the barrier alumina layer containing P was faster than that without P, the slopes of the reciprocal C_b-t_i line changed from the middle stage of immersion. Such differences in dissolution rates have also been reported for pore-widening processes for the fabrication of anodic alumina templates with different pore diameters [51].

The reciprocal C_bs of the remaining five types of AAOs immersed in phosphoric acid for various times were calculated using similar EIS measurements. Additionally, the changes in the obtained reciprocal C_b with the immersion time are summarized in Fig. 7. Because the barrier layer thickness of the Sul-AAO and Oxa-AAO is relatively thin due to their low applied voltages during anodizing (16 V and 35 V), the reciprocal C_b of these AAOs before immersion were measured to be small values of 2.18 $cm^2\mu F^{-1}$ and 3.81 $cm^2\mu F^{-1}$, respectively. Most barrier anodic alumina contained sulfate and oxalate anions originating from the electrolytes used [31,52]. Thus, these AAOs rapidly dissolved in phosphoric acid and the reciprocal C_b became almost zero within approximately 5 min and 7.5 min, respectively. Because the anodizing voltage and corresponding barrier layer thickness of the Eti-AAO were larger than those of the Phos-AAO, the reciprocal C_b of the Eti-AAO before immersion possessed a higher value of 20.6 $cm^2\mu F^{-1}$. Therefore, the complete dissolution time of Eti-AAO (approximately 25 min) was longer than that of Phos-AAO (20 min), despite both exhibiting similar dissolution behaviors. Although the anodizing voltage of Chor-AAO (103 V) was lower than that of Eti-AAO (142 V), the complete dissolution time of Chor-AAO was almost the same as that of Eti-AAO (25 min). The reason for this is that Chro-AAO consists of almost pure alumina without anions, and the dissolution rate of Chro-AAO is relatively slow in phosphoric acid. Compared to these five acidic electrolytes, the reciprocal C_b of Borate-AAO before immersion possessed the highest value of 33.0 $cm^2\mu F^{-1}$. Accordingly, the longest time required for the complete dissolution of Borate-AAO was 45 min. Namely, Borate-AAO possessed the highest chemical resistance in phosphoric acid solutions. Such high chemical resistance may be due to the thick formation of high-purity anodic alumina.

The chemical resistance of Borate-AAO also exhibited the highest value in an alkaline sodium hydroxide solution. The Al specimens covered with the six types of AAO were immersed in a 2.5 M sodium hydroxide solution at 293 K, and the reciprocal C_bs of the AAOs after

immersion for various times were calculated using EIS measurements (Fig. 8). Although the dissolution behavior of the AAOs in the sodium hydroxide solution was similar to that in the phosphoric acid solution, the dissolution rate in the sodium hydroxide solution was much faster because of the high solubility of alumina in the alkaline solution with high pH values and the higher concentration of the solution used [53]. The AAOs formed in the five types of acidic electrolyte solutions completely dissolved in the sodium hydroxide solution within approximately 10 min; in particular, Sul-AAO and Oxa-AAO rapidly disappeared from the Al surface within 1–2 min. In contrast, the Borate-AAO remained until approximately 20 min in the sodium hydroxide solution, thereby exhibiting the highest chemical resistance for the six electrolytes. This complete dissolution time is approximately double that of other AAOs formed in acidic solutions.

There was almost no change in the slope of the linear time variation of reciprocal C_b obtained from the Chro-AAO without anions during immersion in both acidic and alkaline solutions (Figs. 7 and 8). However, the slopes obtained from the Borate-AAO were clearly different in the first and second half periods during immersion. During anodizing aluminum in alkaline sodium tetraborate solution, hydroxide ions may be incorporated into the outer barrier layer. Such differences in chemical composition may cause the change in the slope obtained from the Borate-AAO.

The changes in the time required for the complete dissolution of the barrier layer at the bottom of various AAOs in acidic phosphoric acid (diamond) and alkaline sodium hydroxide (pentagon) solutions with anodizing voltage are summarized in Fig. 9. In both cases of immersion in the acidic and alkaline solutions, the time required for the complete dissolution of the barrier layer of Sul-AAO, Oxa-AAO, Phos-AAO, and Eti-AAO, which were fabricated using typical acidic electrolytes, exhibited a linear relationship. Furthermore, the time required for complete dissolution linearly increased with the anodizing voltage. On the other hand, Chro-AAO exhibited a higher chemical resistance than the linear relationship due to the formation of high-purity anodic alumina without incorporated anions. Notable, Borate-AAO exhibited the highest chemical resistance in both the acidic and alkaline solutions. This is because anodizing in sodium tetraborate led to a large barrier layer thickness per unit anodizing voltage and the formation of high-purity alumina without anions.

4. Conclusions

We experimentally determined the chemical-resistant properties of AAOs formed on the Al surface in 0.52 M phosphoric acid (pH = 1.3) and 2.5 M sodium hydroxide (pH = 13.8) aqueous solutions. AAOs were formed on the Al plates by anodizing using five typical types of acidic electrolytes: sulfuric, oxalic, chromic, phosphoric, and etidronic acids, and alkaline sodium tetraborate. Sul-AAO, Oxa-AAO, Phos-AAO, and Eti-AAO contained incorporated anions in their structures, whereas Chor-AAO and Borate-AAO consisted of pure alumina without any incorporated anions. The barrier layer thickness formed at the bottom of the AAO increased with the anodizing voltage. The time required for the complete dissolution of anion-incorporated AAOs by immersion in both phosphoric acid and sodium hydroxide solutions increased linearly with the anodizing voltage. In addition, Chro-AAO and Borate-AAO exhibited a higher chemical

resistance than the linear relationship due to the formation of high-purity anodic alumina without incorporated anions. As a result, Borate-AAO exhibited the highest chemical resistance owing to the formation of a thick barrier film based on a high anodizing ratio.

Acknowledgments

The authors acknowledge financial support from the Light Metal Educational Foundation, Japan; the Japan Society for the Promotion of Science KAKENHI, Japan (grant numbers:19H02470, 22H01824, 22J11632); and the Nanotechnology Platform Program, Japan (grant number: A-21-HK-0001). We also thank Prof. Hiroki Habazaki, Mr. Satoru Kimura, Dr. Takashi Endo, and Mr. Ryo Oota (Hokkaido University) for their technical support with the GDOES and SEM/STEM observations.

Data availability

Data will be made available on request.

References

1) A. B. Romdhane, D. Veys-Renaux, M. M. NDiaye, S. Bruyère, K. Elleuch, E. Rocca, Anodizing of AS12 alloy in alkaline media, Appl. Surf. Sci. 572 (2022) 151436, https://doi.org/10.1016/j.apsusc.2021.151436.
2) J. Li, H. Wei, K. Zhao, M. Wang, D. Chen, M. Chen, Effect of anodizing temperature and organic acid addition on the structure and corrosion resistance of anodic aluminum oxide films, Thin Solid Films 713 (2020) 138359, https://doi.org/10.1016/j.tsf.2020.138359.
3) M. Mehdizade, M. Soltanieh, A. R. Eivani, Investigation of anodizing time and pulse voltage modes on the corrosion behavior of nanostructured anodic layer in commercial pure aluminum, Surf. Coat. Technol. 358 (2019) 741-752, https://doi.org/10.1016/j.surfcoat.2018.08.046.
4) B. J. Usman, Green and Effective Anodizing of AA 2024-T3 in Methionine-Sulfuric Acid Electrolyte, J. Electrochem. Soc. 169 (2022) 031503, https://doi.org/10.1149/1945-7111/ac565b.
5) H. Asoh, T. Sano, Forming Hard Anodic Films on Aluminum by Anodization in Oxalic Acid and Alcohol, J. Electrochem. Soc. 168 (2021) 103506, https://doi.org/10.1149/1945-7111/ac2ec1.
6) P. Atz-Dick, A. Konrath, Y. R. Melo, C. Radtke, L. F. Dick, Aluminum anodizing with simultaneous silanization for increased hydrophobicity and corrosion protection, Appl. Surf. Sci. 593 (2022) 153392, https://doi.org/10.1016/j.apsusc.2022.153392.
7) Y. Zhang, Y. Chen, G. Bian, Y. Zhang, Electrochemical behavior and corrosion mechanism of anodized 7B04 aluminum alloy in acid NaCl environments, J. Alloys Compd. 886 (2021) 161231, https://doi.org/10.1016/j.jallcom.2021.161231.
8) R. Takeuchi, H. Asoh, Effects of size and position of an unconnected aluminum electrode on bipolar anodization in an AC electric field, Sci. Rep. 11 (2021) 22496, https://doi.org/10.1038/s41598-021-01633-4.
9) T. Kosaba, I. Muto, Y. Sugawara, Galvanic Corrosion of AA5083/Fe in Diluted Synthetic

Seawater: Effect of Anodizing on Local Electrochemistry on and around $Al_6(Fe,Mn)$ on Al-Matrix, J. Electrochem. Soc. 169 (2022) 020550, https://doi.org/10.1149/1945-7111/ac5301.

10) P. Mishra, K. R. Hebert, Self-organization of anodic aluminum oxide layers by a flow mechanism, Electrochim. Acta 340 (2020) 135879, https://doi.org/10.1016/j.electacta.2020.135879.
11) A. Ruiz-Clavijo, O. Caballero-Calero, M. Martín-González, Revisiting anodic alumina templates: From fabrication to applications, Nanoscale 13 (2021) 2227-2265, https://doi.org/10.1039/D0NR07582E.
12) J. T. Domagalski, E. Xifre-Perez, L. F. Marsal, Recent advances in nanoporous anodic alumina: Principles, engineering, and applications, Nanomaterials, 11 (2021) 430, https://doi.org/10.3390/nano11020430.
13) T. Kikuchi, D. Nakajima, O. Nishinaga, S. Natsui, R. O. Suzuki, Porous aluminum oxide formed by anodizing in various electrolyte species, Curr. Nanosci. 11 (2015) 560-571, https://doi.org/10.2174/1573413711999150608144742.
14) W. Lee, S. J. Park, Porous anodic aluminum oxide: anodization and templated synthesis of functional nanostructures, Chem. Rev. 114 (2014) 7487-7556, https://doi.org/10.1021/cr500002z.
15) T. Yanagishita, R. Kawato, H. Masuda, Highly Ordered Anodic Porous Alumina Prepared by Anodization of Al in Extremely Dilute H_2SO_4, J. Electrochem. Soc. 169 (2022) 073504, https://doi.org/10.1149/1945-7111/ac7dc9.
16) A. Poznyak, A. Pligovka, T. Laryn, M. Salerno, Porous alumina films fabricated by reduced temperature sulfuric acid anodizing: Morphology, composition and volumetric growth, Materials 14 (2021) 767, https://doi.org/10.3390/ma14040767.
17) T. Yanagishita, H. Masuda, High-throughput fabrication process for highly ordered through-hole porous alumina membranes using two-layer anodization, Electrochim. Acta 184 (2015) 80-85, https://doi.org/10.1016/j.electacta.2015.10.019.
18) D. Veys-Renaux, N. Chahboun, E. Rocca, Anodizing of multiphase aluminium alloys in sulfuric acid: in-situ electrochemical behaviour and oxide properties, Electrochim. Acta 211 (2016) 1056-1065, https://doi.org/10.1016/j.electacta.2016.06.131.
19) L. Zaraska, K. Syrek, K. Hnida, M. Bobruk, A. Krzysik, T. Łojewski, M. Jaskuła, G. D. Sulka, Nanoporous tin oxides synthesized via electrochemical anodization in oxalic acid and their photoelectrochemical activity, Electrochim. Acta 205 (2016) 273-280, https://doi.org/10.1016/j.electacta.2016.02.023.
20) K. S. Choudhari, S. D Kulkarni, C. Santhosh, S. D. George, Photoluminescence enhancement and morphological properties of nanoporous anodic alumina prepared in oxalic acid with varying time and temperature, Microporous Mesoporous Mater. 271 (2018) 138-145, https://doi.org/10.1016/j.micromeso.2018.06.004.
21) L. Zaraska, M. Jaskuła, G. D. Sulka, Porous anodic alumina layers with modulated pore diameters formed by sequential anodizing in different electrolytes, Mater. Lett. 171 (2016) 315-318, https://doi.org/10.1016/j.matlet.2016.02.113.
22) A. Gasco-Owens, D. Veys-Renaux, V. Cartigny, E. Rocca, Large-pores anodizing of 5657

aluminum alloy in phosphoric acid: An in-situ electrochemical study, Electrochim. Acta 382 (2021) 138303, https://doi.org/10.1016/j.electacta.2021.138303.
23) L. Zaraska, G. D. Sulka, M. Jaskuła, The effect of n-alcohols on porous anodic alumina formed by self-organized two-step anodizing of aluminum in phosphoric acid, Surf. Coat. Technol. 204 (2010) 1729-1737, https://doi.org/10.1016/j.surfcoat.2009.10.051.
24) X. Zhu, Y. Song, D. Yu, C. Zhang, W. Yao, A novel nanostructure fabricated by an improved two-step anodizing technology, Electrochem. Commun. 29 (2013) 71-74, https://doi.org/10.1016/j.elecom.2013.01.018.
25) D. Elabar, A. Němcová, T. Hashimoto, P. Skeldon, G. E. Thompson, Effect of sulphate impurity in chromic acid anodizing of aluminium, Corr. Sci. 100 (2015) 377-385, https://doi.org/10.1016/j.corsci.2015.08.019.
26) D. Elabar, T. Hashimoto, P. Skeldon, G. E. Thompson, Effect of low levels of sulphate on the current density and film morphology during anodizing of aluminium in chromic acid, Electrochim. Acta 196 (2016) 206-222, https://doi.org/10.1016/j.electacta.2016.01.230.
27) T. Kikuchi, M. Yamashita, M. Iwai, R. O. Suzuki, Self-ordering of porous anodic alumina fabricated by anodizing in chromic acid at high temperature, J. Electrochem. Soc. 168 (2021) 093501, https://doi.org/10.1149/1945-7111/ac2101.
28) M. Iwai, T. Kikuchi, R. O. Suzuki, S. Natsui, Electrochemical and morphological characterization of porous alumina formed by galvanostatic anodizing in etidronic acid, Electrochim. Acta 320 (2019) 134606, https://doi.org/10.1016/j.electacta.2019.134606.
29) M. Iwai, T. Kikuchi, R. O. Suzuki, High-speed galvanostatic anodizing without oxide burning using a nanodimpled aluminum surface for nanoporous alumina fabrication, Appl. Surf. Sci. 537 (2021) 147852, https://doi.org/10.1016/j.apsusc.2020.147852.
30) T. Kikuchi, A. Takenaga, S. Natsui, R. O. Suzuki, Advanced hard anodic alumina coatings via etidronic acid anodizing, Surf. Coat. Technol. 326 (2017) 72-78, https://doi.org/10.1016/j.surfcoat.2017.07.043.
31) G. E. Thompson, G. C. Wood, Porous anodic film formation on aluminium, Nature 290 (1981) 230-232, https://doi.org/10.1038/290230a0.
32) S. Ono, Nanostructure Analysis of Anodic Films Formed on Aluminum-Focusing on the Effects of Electric Field Strength and Electrolyte Anions, Molecules 26 (2021) 7270, https://doi.org/10.3390/molecules26237270.
33) S. Z. Chu, K. Wada, S. Inoue, M. Isogai, Y. Katsuta, A. Yasumori, Large-scale fabrication of ordered nanoporous alumina films with arbitrary pore intervals by critical-potential anodization, J. Electrochem. Soc. 153 (2006) B384-B391, https://doi.org/10.1149/1.2218822.
34) A. M. Brudzisz, D. Giziński, W. J. Stępniowski, Incorporation of ions into nanostructured anodic oxides—Mechanism and functionalities, Molecules 26 (2021) 6378, https://doi.org/10.3390/molecules26216378.
35) Ö. Ö. Çapraz, Q. van Overmeere P. Shrotriya, K. R. Hebert, Stress induced by electrolyte anion incorporation in porous anodic aluminum oxide, Electrochim. Acta 238 (2017) 368-374, https://doi.org/10.1016/j.electacta.2017.04.014.
36) S. Akiya, T. Kikuchi, S. Natsui, N. Sakaguchi, R. O. Suzuki, Self-ordered porous alumina

fabricated via phosphonic acid anodizing, Electrochim. Acta 190 (2016) 471-479, https://doi.org/10.1016/j.electacta.2015.12.162.
37) M. Iwai, T. Kikuchi, R. O. Suzuki, Initial Structural Changes of Porous Alumina Film via High-Resolution Microscopy Observations, ECS J. Solid State Sci. Technol. 9 (2020) 044004, https://doi.org/10.1149/2162-8777/ab89ba.
38) T. Kikuchi, Y. Suzuki, M. Iwai, R. O. Suzuki, Anodizing aluminum and its alloys in etidronic acid to enhance their corrosion resistance in a sodium chloride solution, J. Electrochem. Soc. 167 (2020) 121502, https://doi.org/10.1149/2.0221912jes.
39) Y. Suzuki, K. Kawahara, T. Kikuchi, R. O. Suzuki, S. Natsui, Corrosion-resistant porous alumina formed via anodizing aluminum in etidronic acid and its pore-sealing behavior in boiling water, J. Electrochem. Soc. 166 (2019) C261-C269, https://doi.org/10.1149/2.0221912jes.
40) M. Iwai, T. Kikuchi, R. O. Suzuki, Self-ordered nanospike porous alumina fabricated under a new regime by an anodizing process in alkaline media, Sci. Rep. 11 (2021) 7240, https://doi.org/10.1038/s41598-021-86696-z.
41) T. Kikuchi, K. Kunimoto, H. Ikeda, D. Nakajima, R. O. Suzuki, S. Natsui, Fabrication of anodic porous alumina via galvanostatic anodizing in alkaline sodium tetraborate solution and their morphology, J. Electroanal. Chem. 846 (2019) 113152, https://doi.org/10.1016/j.jelechem.2019.05.034.
42) M. Iwai, T. Kikuchi, Fabrication of unique porous alumina films with extremely high porosity and an ultra-flat barrier layer by anodizing aluminum in sodium metaborate, Electrochim. Acta 399 (2021) 139440, https://doi.org/10.1016/j.electacta.2021.139440.
43) T. Kikuchi, M. Sato, M. Iwai, D. Nakajima, J. Nunomura, Y. Oya, S. Natsui, Formation of Bright White Plasma Electrolytic Oxidation Films with a Uniform Maze-Like Structure by Anodizing Aluminum in Ammonium Tetraborate Solutions, J. Electrochem. Soc. 169 (2022) 043505, https://doi.org/10.1149/1945-7111/ac62bc.
44) T. Kikuchi, T. Taniguchi, R. O. Suzuki, S. Natsui, Fabrication of a plasma electrolytic oxidation/anodic aluminum oxide multi-layer film via one-step anodizing aluminum in ammonium carbonate, Thin Solid Films 697 (2020) 137799, https://doi.org/10.1016/j.tsf.2020.137799.
45) A. Terashima, M. Iwai, T. Kikuchi, Nanomorphological changes of anodic aluminum oxide fabricated by anodizing various phosphate solutions over a wide pH range, Appl. Surf. Sci. 605 (2022) 154687, https://doi.org/10.1016/j.apsusc.2022.154687.
46) W. Sun, Y. Liu, T. Li, S. Cui, S. Chen, Q. Yu, D. Wang, Anti-corrosion of amphoteric metal enhanced by MAO/corrosion inhibitor composite in acid, alkaline and salt solutions, J. Colloid Interface Sci. 554 (2019) 488-499, https://doi.org/10.1016/j.jcis.2019.07.035.
47) M. García-Rubio, P. Ocón, M. Curioni, G.E. Thompson, P. Skeldon, A. Lavía, I. García, Degradation of the corrosion resistance of anodic oxide films through immersion in the anodising electrolyte, Corr. Sci. 52 (2010) 2219-2227, https://doi.org/10.1016/j.corsci.2010.03.004.
48) S. Hirai, K. Shimakage, S. Aizawa, K. Wada, Alkaline Corrosion Resistance of Anodized

Aluminum Coated with Zirconium Oxide by a Sol-Gel Process, J. Am. Ceram. Soc. 81 (1998) 3087-3092, https://doi.org/10.1111/j.1151-2916.1998.tb02742.x.
49) J. Oh, C. V. Thompson, Abnormal anodic aluminum oxide formation in confined structures for lateral pore arrays, J. Electrochem. Soc. 158 (2011) C71-C75, https://doi.org/10.1149/1.3532778.
50) S. Akiya, T. Kikuchi, S. Natsui, R. O. Suzuki, Nanostructural characterization of large-scale porous alumina fabricated via anodizing in arsenic acid solution, Appl. Surf. Sci. 403 (2017) 652-661, https://doi.org/10.1016/j.apsusc.2017.01.243.
51) H. Han, S. J. Park, J. S. Jang, H. Ryu, K. J. Kim, S. Baik, W. Lee, In situ determination of the pore opening point during wet-chemical etching of the barrier layer of porous anodic aluminum oxide: nonuniform impurity distribution in anodic oxide, ACS Appl. Mater. Interfaces 5 (2013) 3441-3448, https://doi.org/10.1021/am400520d.
52) R. Kondo, T. Kikuchi, S. Natsui, R. O. Suzuki, Fabrication of self-ordered porous alumina via anodizing in sulfate solutions, Mater. Lett. 183 (2016) 285-289, https://doi.org/10.1016/j.matlet.2016.07.109.
53) C. Vargel, Corrosion of Aluminum, 1st ed., Elsevier Science, Amsterdam, 2004.

Captions

Table 1 Anodizing behaviors and structural parameters of the AAO fabricated by anodizing in different electrolyte solutions.

Fig. 1 Changes in the voltage, U_a, with time, t_a, during galvanostatic anodizing of Al in 0.3 M sulfuric acid (293 K), 0.3 M oxalic acid (293 K), 0.3 M chromic acid (313 K), 0.3 M phosphoric acid (293 K), 0.3 M etidronic acid (313 K), and 0.3 M sodium tetraborate (333 K) solutions at a constant current density of 40 Am^{-2} for 60 min.

Fig. 2 Scanning electron microscopy (SEM) images of the fracture cross-section of the anodic aluminum oxide (AAO) films formed by anodizing in sulfuric acid, oxalic acid, phosphoric acid, etidronic acid, chromic acid, and sodium tetraborate solutions at 40 Am^{-2} for 60 min.

Fig. 3 Glow discharge optical emission spectrometry (GD-OES) elemental depth profiles of AAOs formed by anodizing in sulfuric acid, oxalic acid, phosphoric acid, etidronic acid, chromic acid, and sodium tetraborate solutions at 40 Am^{-2} for 60 min.

Fig. 4 a) Bode diagrams of the Al specimen covered with the Phos-AAO and the electropolished Al specimen before and after immersion in a 0.52 M phosphoric acid solution at 333 K. The electrochemical impedance spectroscopy (EIS) measurements were performed in a neutral 0.5 M boric acid/ 0.05 M sodium tetraborate solution. b) A schematic model of the equivalent circuit of the AAO-covered Al surface.

Fig. 5 Change in the reciprocal capacitance of the Phos-AAO-covered Al specimen, C_b, with the immersion time, t_i, in a 0.52 M phosphoric acid solution at 333 K.

Fig. 6 a) SEM images of the surface and cross-section of the Phos-AAO-covered Al specimen after immersion in a 0.52 M phosphoric acid solution at 333 K for 7-20 min. b) Scanning transmission electron microscopy and energy dispersive X-ray spectroscopy (STEM-EDS) elemental distribution maps of the Phos-AAO before and after immersion for 7-15 min.

Fig. 7 Changes in the reciprocal capacitance of the a) Sul-AAO, Oxa-AAO, Phos-AAO, and Eti-AAO, and b) Chro-AAO and Borate-AAO-covered Al specimen, C_b, with the immersion time, t_i, in a 0.52 M phosphoric acid solution at 333 K.

Fig. 8 Changes in the reciprocal capacitance of the a) Sul-AAO, Oxa-AAO, Phos-AAO, and Eti-AAO, and b) Chro-AAO and Borate-AAO-covered Al specimen, C_b, with the immersion time, t_i, in a 2.5 M sodium hydroxide solution at 293 K.

Fig. 9 Changes in the time required for the complete dissolution of the barrier layer at the bottom of various AAOs in a 0.52 M acidic phosphoric acid solution at 333 K (diamond) and a 2.5 M alkaline sodium hydroxide solution at 293 K (pentagon) with the anodizing voltage. The pink and purple lines indicate the complete dissolution time in the acidic and alkaline solutions, respectively.

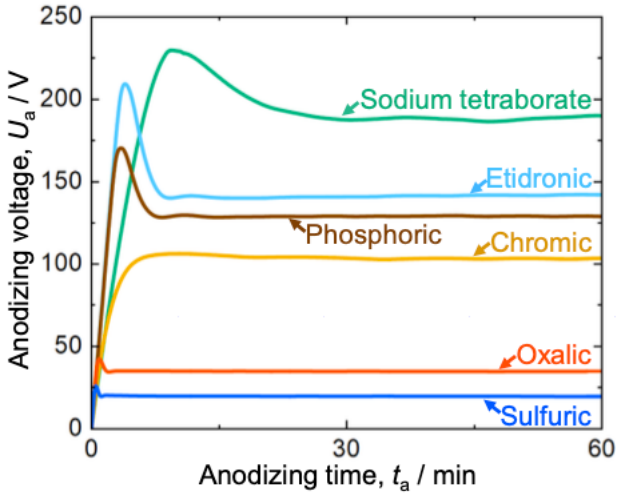

Figure 1

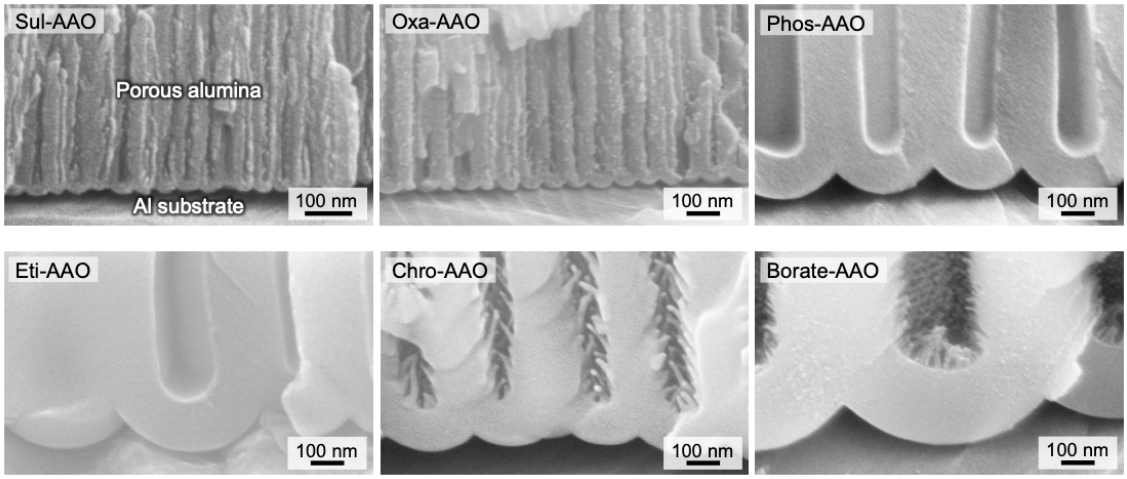

Figure 2

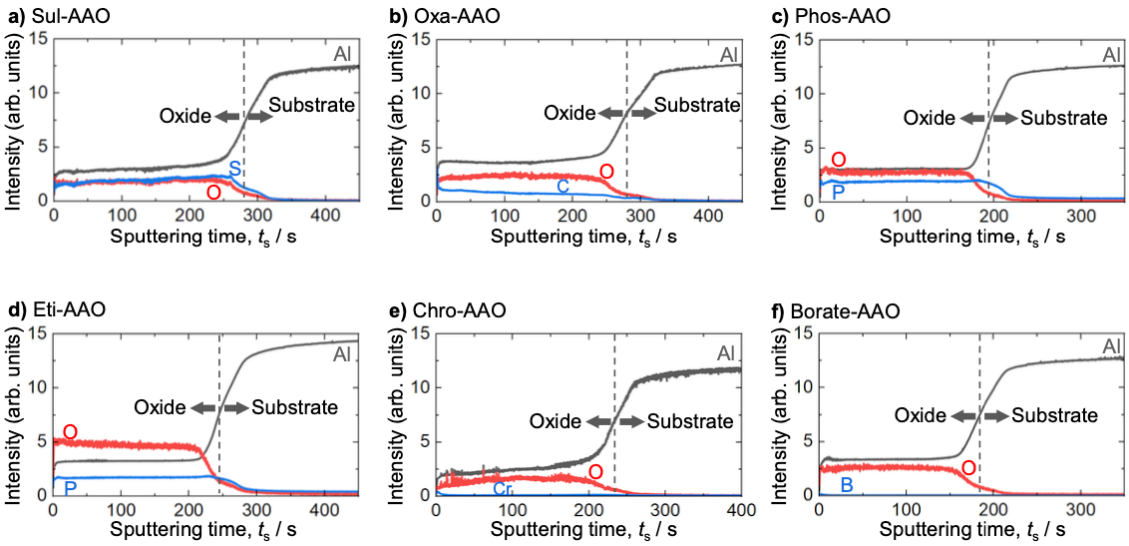
a) Sul-AAO
b) Oxa-AAO
c) Phos-AAO
d) Eti-AAO
e) Chro-AAO
f) Borate-AAO
Intensity (arb. units)
Sputtering time, t_s / s
Oxide
Substrate
Al
O
S
C
P
Cr
B

Figure 3

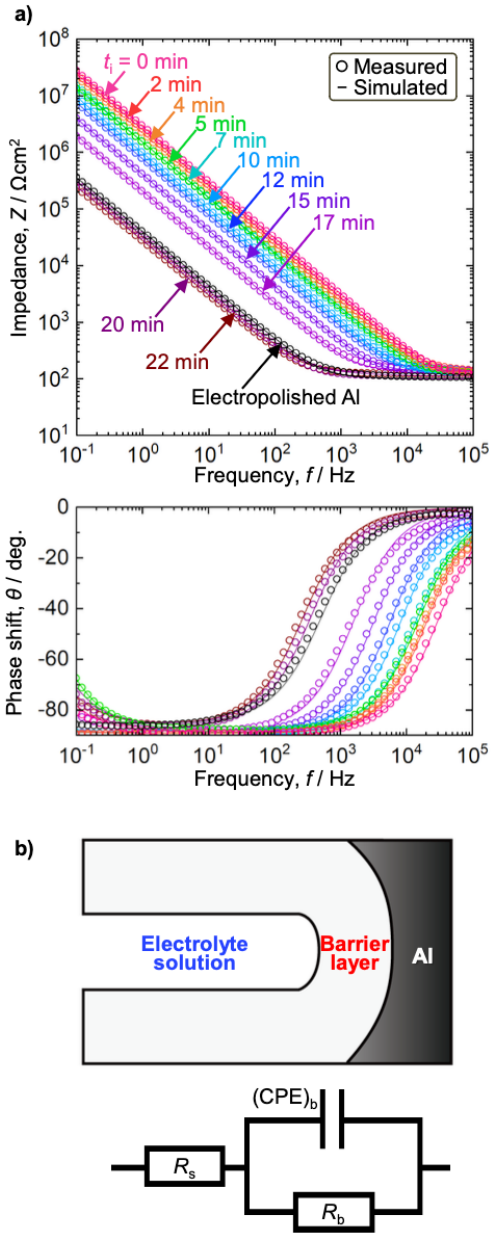
a)
Measured
Simulated
t_i = 0 min
2 min
4 min
5 min
7 min
10 min
12 min
15 min
17 min
20 min
22 min
Electropolished Al
Impedance, Z / Ωcm²
Frequency, f / Hz
Phase shift, θ / deg.
Frequency, f / Hz
b)
Electrolyte solution
Barrier layer
Al
(CPE)b
Rs
Rb

Figure 4

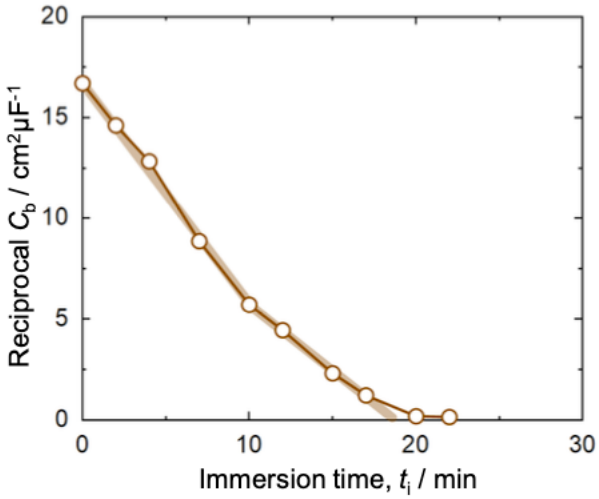
20
15
10
5
0
0
10
20
30
Reciprocal C_b / cm^{2}µF^{-1}
Immersion time, t_i / min

Figure 5

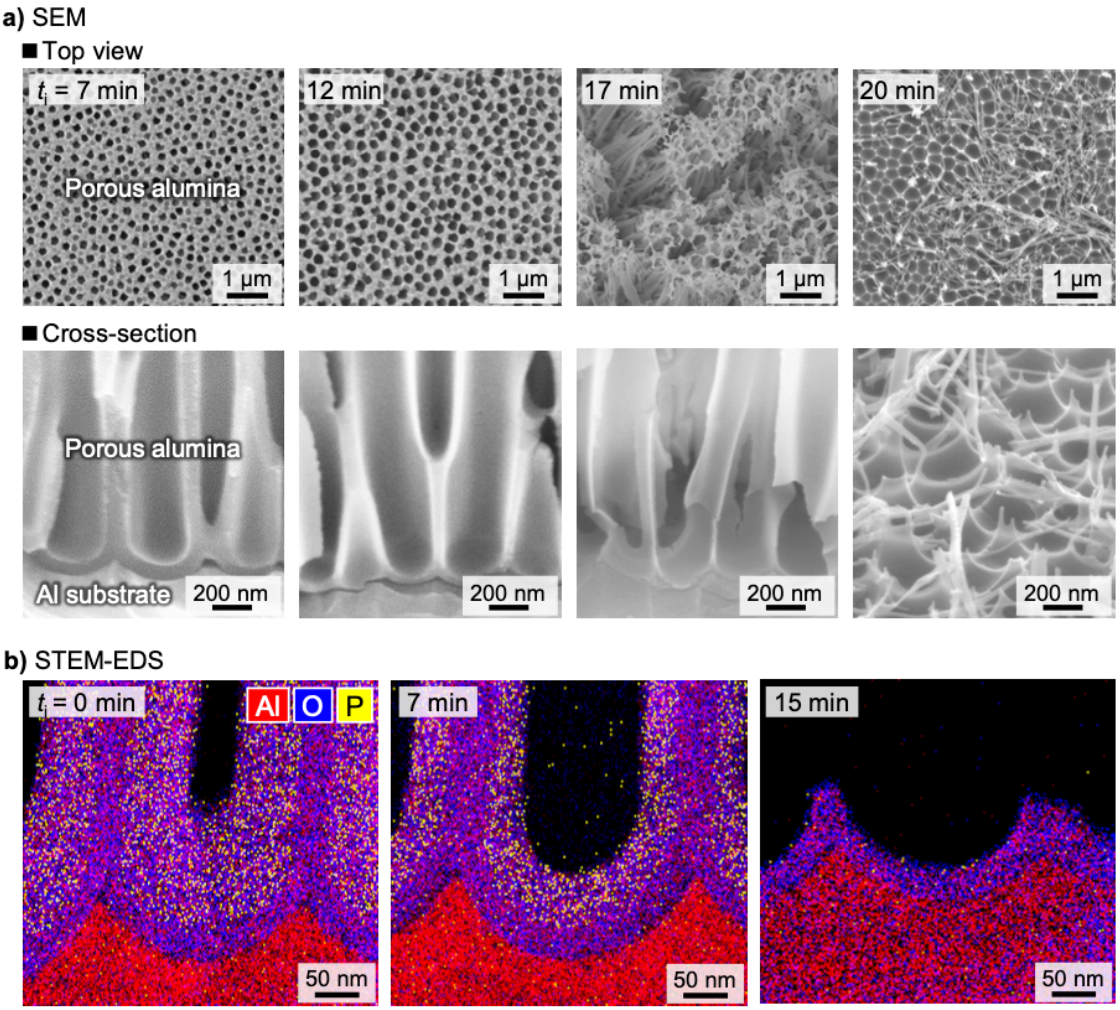
a) SEM
Top view
t_i = 7 min
Porous alumina
1 μm
12 min
1 μm
17 min
1 μm
20 min
1 μm
Cross-section
Porous alumina
Al substrate
200 nm
200 nm
200 nm
200 nm
b) STEM-EDS
t_i = 0 min
Al
O
P
50 nm
7 min
50 nm
15 min
50 nm

Figure 6

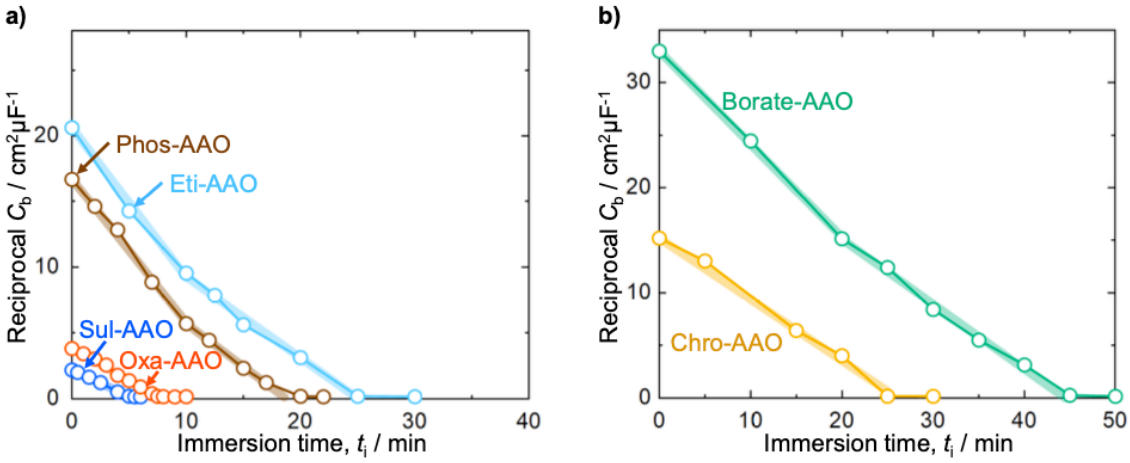

Figure 7

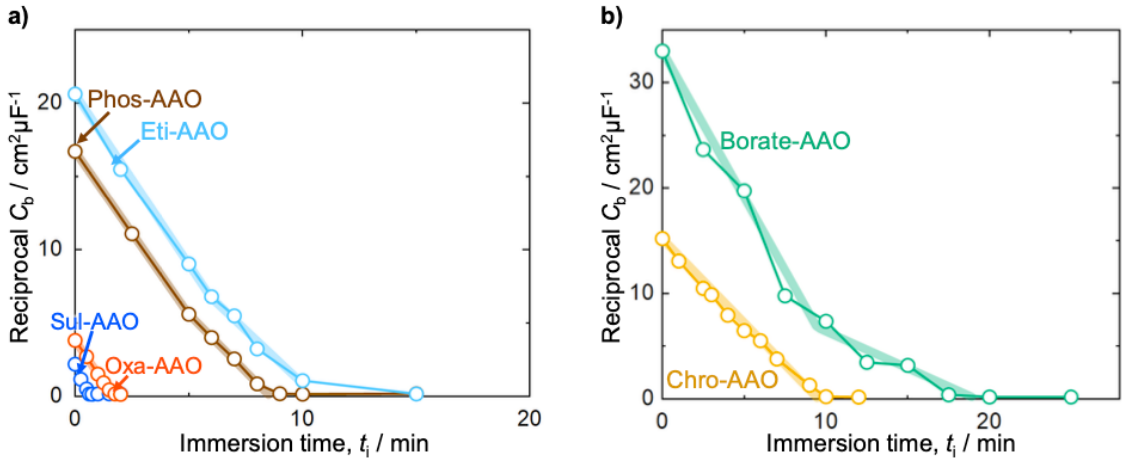

Figure 8

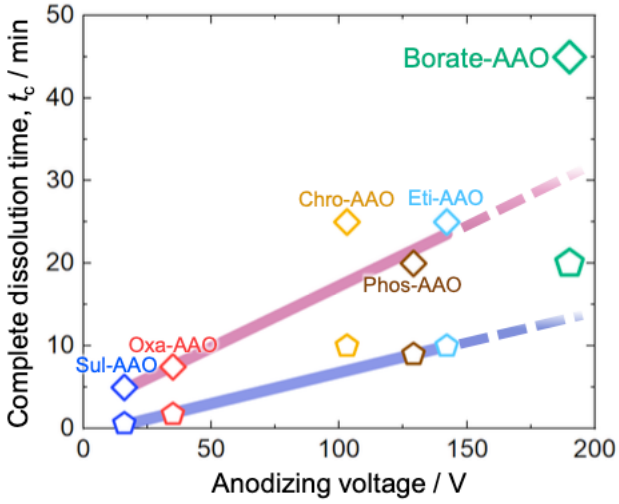
Complete dissolution time, t_c / min
Anodizing voltage / V
Borate-AAO
Chro-AAO
Eti-AAO
Phos-AAO
Oxa-AAO
Sul-AAO
0
10
20
30
40
50
0
50
100
150
200

Figure 9